Optical hydrography for seasonal and flood-induced changes in aquatic vegetation

Jan Rhomberg-Kauert[1], Lucas Dammert[1], Michael Grömer[2], Martin Pfennigbauer[3] and Gottfried Mandlburger[1]

[1]Department of Geodesy and Geoinformation, TU Wien; 1040 Vienna, Austria - jan.rhomberg-kauert@geo.tuwien.ac.at, lucas.dammert@geo.tuwien.ac.at, gottfried.mandlburger@geo.tuwien.ac.at
[2]VERBUND Hydro Power GmbH; 1150 Wien, Austria - michael.groemer@verbund.com
[3]*RIEGL* Research and Defense GmbH; 3480 Horn, Austria - mpfennigbauer@riegl.com

Keywords: laser bathymetry, imaging, macrophytes, extreme weather events, seasonal changes, extinction

Abstract

The increasing occurrence of extreme weather events has a far reaching impact on all types of ecosystems. This includes submerged ecosystems, where floods and droughts influence the flora and fauna. Monitoring such submerged landscapes and their aquatic vegetation has gained interest in recent decades, and advances in remote sensing technology allow detailed mapping of those ecosystems. There, changes in vegetation extent throughout such extreme weather events remain insufficiently quantified, as comprehensive data sets before and after extreme weather events are rarely obtained. Thus, this study presents an extensive case study for a vegetated pond in Lower Austria, which was subjected to major flooding during the September 2024 flood in Austria. The presented data set includes aerial imaging and bathymetric LiDAR data for six epochs over three years, four before the flood and two after. This study presents the near-extinction of the submerged vegetation after the flood event and puts the results into perspective with the seasonal changes before the flood. For the three half-year periods before the flood event, the height of the vegetation shows a median fluctuation between $-0.3\,\mathrm{m}$ to $1\,\mathrm{m}$ over the pond, while the change in vegetation height after the flood event has a median value of approximately $-2.9\,\mathrm{m}$. Although the seasonal changes are in alignment with the expected values, based on current research regarding the type of macrophytes present in the study area, the post-flood changes present a significant decrease in the overall vegetation. This, along with changes in turbidity, indicates a long-term impact on the pond and outlines the impact of extreme weather events on aquatic ecosystems. In general, the case study presents insights into rarely documented changes due to extreme weather events and provides a remote sensing approach to quantify changes in aquatic landscapes.

1. Introduction

The analysis of aquatic habitats is crucial to understanding submerged ecosystems and has a long history in different fields of research (Mandlburger et al., 2013; Murphy et al., 2018; Ostendorp et al., 2003; Rowan and Kalacska, 2021). To monitor the state and changes of aquatic ecosystems, several approaches have been introduced and tested over the last decades (Mandlburger et al., 2023; Rowan and Kalacska, 2021). In the field of remote sensing, both imaging and LiDAR have become widely used techniques (Mandlburger, 2022).

For imaging, the advancement of unmanned areal vehicles (UAVs) has allowed large-scale, cost-effective studies of all types of habitats (Ventura et al., 2017). This also applies to aquatic vegetation, as image data can be used in clear water to monitor vegetation expansion at low costs (Kellaris et al., 2019; Chabot et al., 2018). A down side of airborne imagining is that it requires clear water and spatial information is limited to the canopy of vegetation, which reduces spatial information for submerged terrain often obstructed by lower layers of dense vegetation (Mandlburger, 2022).

This is where bathymetric LiDAR can improve the spatial coverage of the mapped aquatic ecosystem, as advances in the last decades have improved depth penetration (around 2 Secchi depths) (Mandlburger et al., 2023; Schwarz et al., 2019) and allow for complex vegetation analysis (Rhomberg-Kauert et al., 2024; Wagner et al., 2024). Here, in particular, the use of full-waveform LiDAR allows the application of algorithms tailored for underwater data to the recorded waveform, thus improving water surface detection and allowing deeper bottom echo extraction (Schwarz et al., 2017, 2019; Pfennigbauer et al., 2020). Furthermore, through the combination of multiple waveforms (waveform averaging), deeper depth penetration can be achieved as the signal-to-noise ratio is improved, and therefore deeper bottom echos can be detected, but at the cost of lower spatial resolution within the vegetation, as small-scale features can potentially be smoothed out (Mader et al., 2021; Mandlburger et al., 2023). The downside of bathymetric LiDAR systems is the high cost of such systems and the requirements regarding the operating platform, since large-scale UAVs with special permits are required or manned airborne systems must be used (Mandlburger, 2022).

Optical remote sensing has been shown to be well suited for mapping macrophyte populations (Rhomberg-Kauert et al., 2024; Schumacher et al., 2024) enabling change detection by repeated surveys of the same area (Mandlburger et al., 2015). Alternatively, such studies can be carried out by diving teams or using SONAR (Lønborg et al., 2021; Mandlburger, 2022). Diver-based surveys vary in repeatability and are often time consuming (Lønborg et al., 2021). Multibeam SONAR is generally suitable for mapping macrophyte populations in water bodies of sufficient depth (Lønborg et al., 2021; Mandlburger, 2022). However, for both SONAR and LiDAR, the initial costs are often a limiting factor (Lønborg et al., 2021). For SONAR, depending on the height of the vegetation, the survey vessel could impact the ecosystem during measurement (Eriksson et al., 2004). Therefore, for non-fully submerged macrophytes and clear shallow waters, airborne optical remote sensing offers a suitable tool for surveying aquatic vegetation (Lønborg et al., 2021; Rhomberg-Kauert et al., 2024).

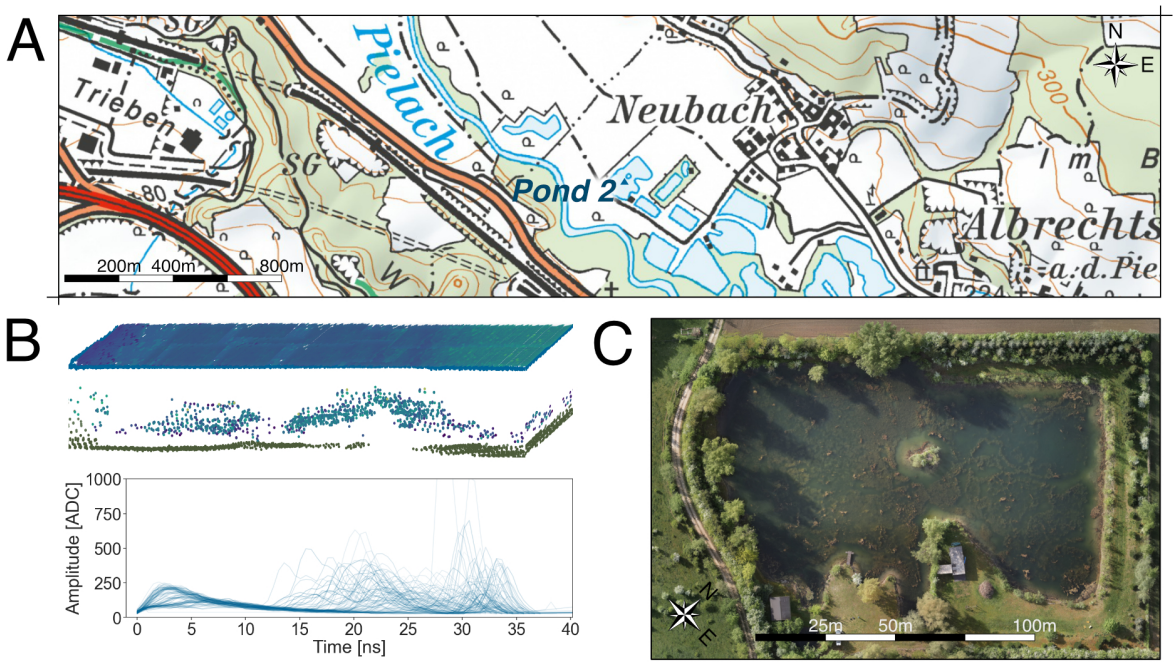

Figure 1. Map overview of the study area near Loosdorf, Lower Austria (48.2166 N, 15.3744 E), with the survey pond marked as Pond 2 (BEV, 2024). (B) Illustration of the acquired point cloud and full-waveform data. (C) Orthophoto of the pond in April 2024.

Detection of changes and quantification of ecosystem parameters are among the most important applications of all types of aquatic landscape monitoring techniques. This includes monitoring seasonal changes in macrophyte populations and extends to documenting the impact of extreme weather events on submerged vegetation (Schmieder et al., n.d.). In the recent past, the occurrence of extreme weather events, such as flooding and drought, has increased (Blöschl et al., 2018). A major flooding event was the century flood in Austria in September 2024 (Blöschl, 2024), which included the area of Loosdorf and the Pielach River in Lower Austria. There, previous studies have documented flood events in the past (Mandlburger et al., 2015), and in general, the area is well surveyed, including a set of ponds, of which a subset is vegetated.

For the study, we compared six epochs between August 2022 and February 2025. Four of these epochs are before the flood event, and two after. Each epoch is surveyed by both bathymetric LiDAR and aerial imaging, and the seasonal changes can be analyzed both visually and, for the LiDAR data, quantitatively. We first introduce the study site in general, as well as all the data sets acquired during the six measurement campaigns (Section 2). Secondly, the data annotation methodology and the software used are introduced, together with the selected approach to change detection (Section 3). Based on the data and the change detection method, comprehensive results are given for vegetation extent (Section 4.1), seasonal changes (Section 4.2) and flood-induced changes (Section 4.3). These are then critically discussed (Section 5) and lastly a conclusion of the gained insight is given (Section 6).

2. Materials

To analyze the changes between different epochs of aquatic vegetation data, we first introduce the study site and present the data sets for each epoch.

2.1 Study site

The surveyed area is located near Loosdorf, Lower Austria. There, the region encompasses the pre-Alpine Pielach River and about a dozen freshwater ponds in the adjacent flood plain. A subset of the ponds, including the focus of our study, Pond 2, contains submerged vegetation, which can be seen in the orthophoto resulting from the survey in April 2024 (Figure 1).

2.2 LiDAR data

The LiDAR data for the study were surveyed using two topo-bathymetric LiDAR systems, primarily a *RIEGL* VQ-880-GII and for the last epoch a *RIEGL* VQ-840-GL. For Epochs 1-5, the LiDAR system was deployed from an aircraft, and for Epoch 6 the system was mounted on a helicopter. The average

Epoch	Date	Sensor	Range [m]	Wavelength [nm]	Frequency [kHz]	Beam divergence [mrad]
1	24.08.2022	*RIEGL* VQ-880-GII	650	532	200	0.9
2	08.02.2023	*RIEGL* VQ-880-GII	746	532	550	1.3
3	13.09.2023	*RIEGL* VQ-880-GII	704	532	200	0.9
4	30.04.2024	*RIEGL* VQ-880-GII	692	532	550	2.0
5	09.10.2024	*RIEGL* VQ-880-GII	705	532	550	1.3
6	11.02.2025	*RIEGL* VQ-840-GL	164	532	100	3.0

Table 1. Parameters for the airborne laser scanning data acquisitions.

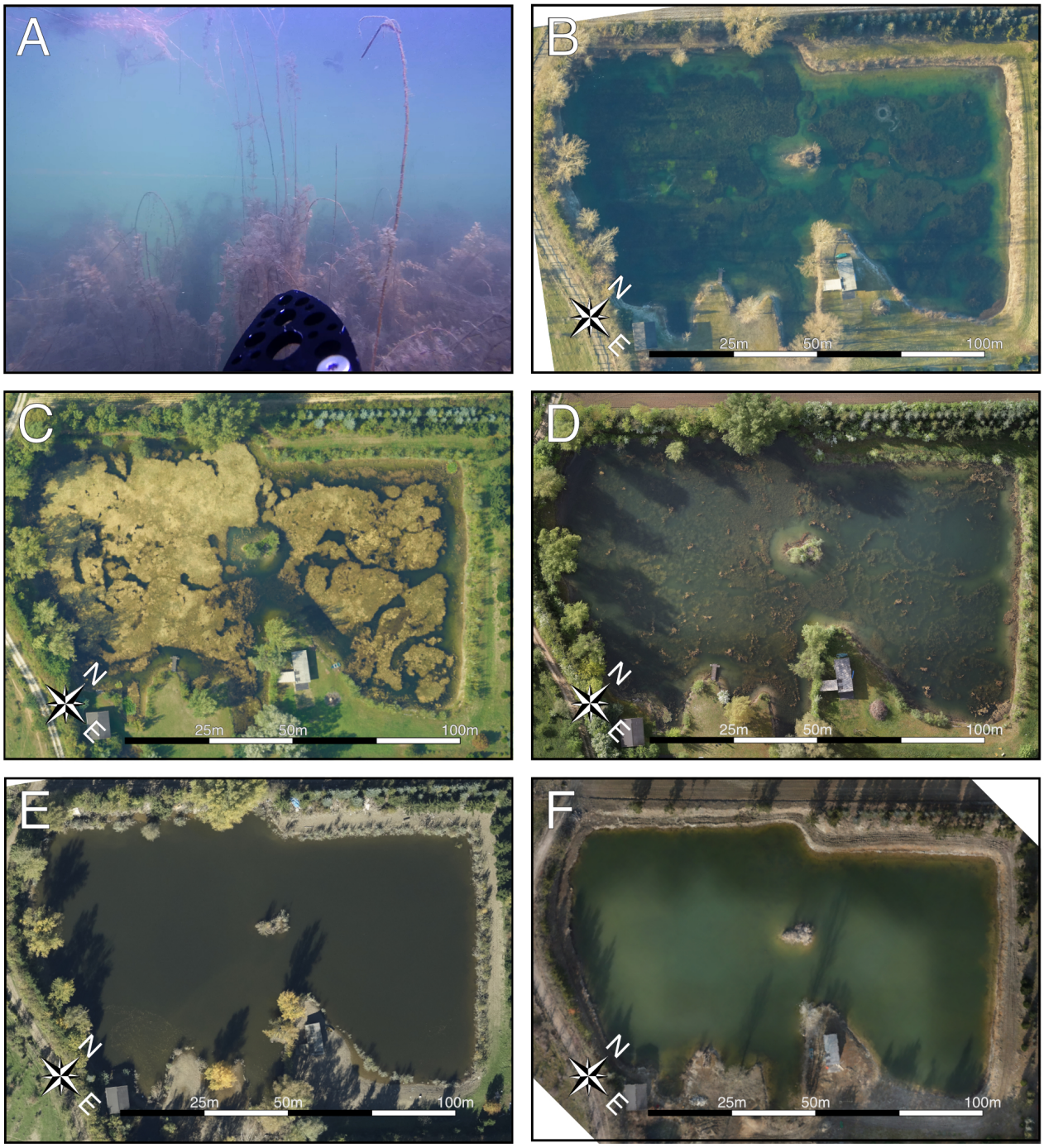

Figure 2. ROV underwater image and image data for Epochs 2-6 of the presented study. (A) ROV image, Spring 2024 (B) Epoch 2, Winter 2022/2023 (C) Epoch 3, Autumn 2023, (D) Epoch 4, Spring 2024, (E) Epoch 5, Autumn 2024 (F) Epoch 6, Winter 2024/2025

ranges and system configurations are shown in Table 1. Both systems are capable of recoding the full waveform. Furthermore, in post-processing the point cloud data was extracted using the Surface-Volume-Bottom algorithm (SVB) of Schwarz et al. (2019). Lastly, to compare all the data sets, the data recorded was exported as a point cloud (Figure 1) in LAS format in a georeferenced coordinate system (ETRS89, UTM33; EPSG: 25833), based on kinematic GNSS processing.

2.3 Image data

To visually capture vegetation changes, high-resolution aerial images were used to generate orthophotos of the surveyed area (Figure 2). In addition, for a single epoch (Spring 2024, Figure 2A) underwater images were acquired using a remotely operated vehicle (ROV). For Epoch 1, no image data is available. In Epochs 2, 3, and 5, nadir images were used, as the system of these surveys is equipped with a $50\,\mathrm{mm}$ focal length camera (*RIEGL*-CS6) capable of taking up to $100\,\mathrm{MPixel}$ images using a medium format sensor. For Epochs 4 and 6, the image data were acquired with a DJI Zenmuse P1 $45\,\mathrm{MPixel}$ RGB

camera and combined into an orthophoto with a resolution of 5 cm per pixel. In our study, the image data are used solely for visual inspection, and thus we do not describe our georeferencing strategy.

3. Method

Comparison of the LiDAR data sets requires three processing steps. First, the data need to be annotated (Section 3.1), afterwards a digital terrain model (DTM) of the pond and a digital surface model (DSM) of the vegetation are derived (Section 3.2) and lastly these models are used to map the vegetation extent for each epoch and extract inter-epoch changes (Section 3.3).

3.1 Data annotation

Data annotation was carried out in alignment with the images of each epoch, providing a reference for where water surface data and floating vegetation differ (Figure 2). For the manual annotation, the software add-on PointCloudLabeler[1] from the OPALS (Version 2.6.0) point cloud processing software (Pfeifer et al., 2014) was used. This tool allows the user to annotate the point cloud data in transects perpendicular to a digitized 2D axis. The transect is chosen so that the width covers the entire pond (120 m) and has an extent of 3 m along the 2D axis. Using this approach, each epoch is iteratively annotated. We differentiate the point cloud into three distinct classes, namely, terrain, vegetation, and water. These classes build the basis for the processing steps described in the next section, where the point cloud is split based on the annotation, and the vegetation and terrain are further analyzed.

3.2 Terrain and surface models

From the annotated point cloud we can now extract different terrain and surface models. To extract vegetation height, first a DTM has to be calculated from the terrain points. As dense vegetation often obstructs bottom echoes, and especially the dense vegetation in autumn is almost impenetrable for the LiDAR system, we used the waveform averaged point cloud from the Winter 2024/2025 measurements to calculate a DTM. This data set yielded an almost complete coverage of the pond, and thus a DTM with a regular grid spacing of 4 m can be calculated. Here, we assume that the flood did not significantly change the terrain of the ponds, which is later discussed among the other assumptions (Section 5.1).

The DTM is generated using the DTM module of the OPALS software (Pfeifer et al., 2014). The module is used with standard parameters and a grid size of 4 m. In more detail, during processing, a linear functional model (tilted planes) is used. For each grid point, the points within the defined neighborhood are used to locally fit a plane, and the grid height is calculated from the resulting plane parameters. In contrast to DTM, DSMs were calculated individually for each epoch using the landscape-dependent DSM calculation approach (Hollaus et al., 2010) implemented in the DSM module of the OPALS software (Pfeifer et al., 2014). In areas with a high vertical point cloud spread, the algorithm selects the maximum height for each cell of a regular raster. In smooth areas, the grid height is calculated from a best-fitting plane. In case of low point density, void grid cells can occur, which are set to zero in our case. The grid size parameter for the DSMs is set to 1 m to obtain continuous coverage without loss of detail. The input data for each DSM consist of only the vegetation, with the exception of Epochs 5 and 6, as for these epochs, not enough vegetation was detected to successfully compute a DSM. In these two cases, the DSM therefore consists of vegetation points combined with the terrain points of the Epoch 6 (the DTM points). Thus, the DSM for the last two epochs contains also surface points, but is identical in those to the DTM. In order to compare the individual DSMs and calculate the vegetation height in relation to the DTM,

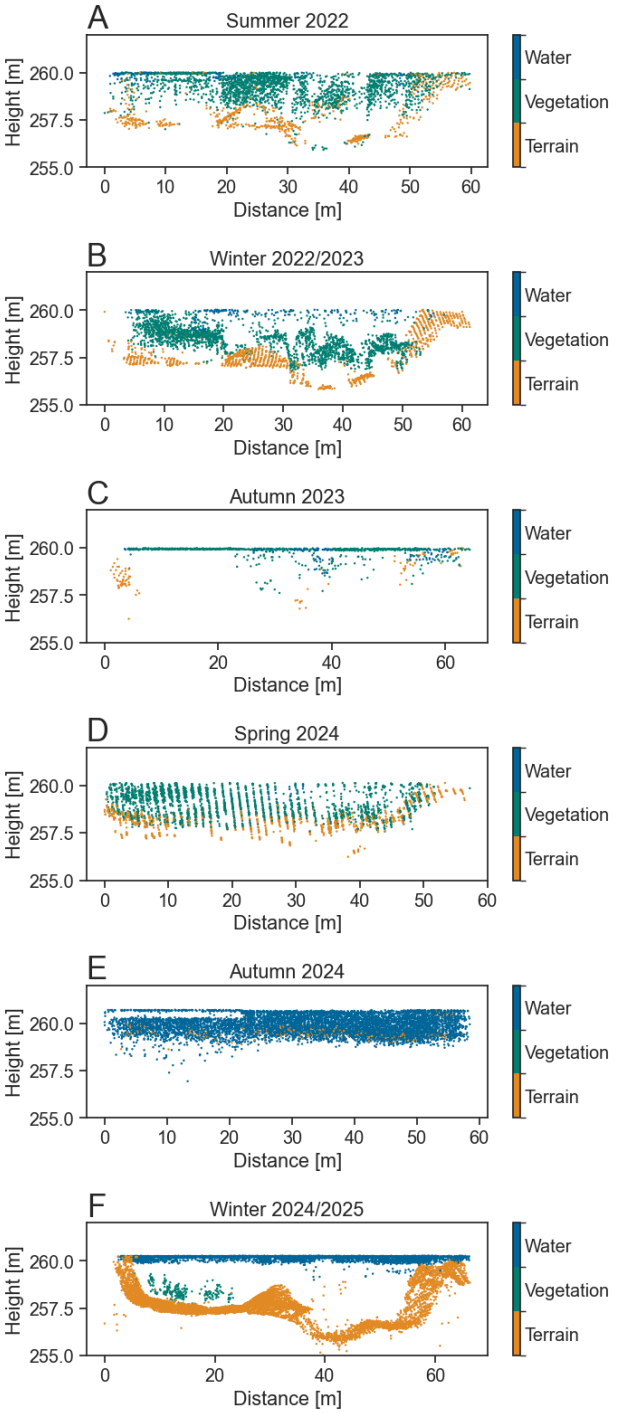

Figure 3. A selected cross-section of the pond shown in Figure 1 for each measurement campaign over the last three years, with manually annotated labels.

[1] https://github.com/TUW-GEO/opals_PointCloudLabeler

3.3 Change detection

we leverage change detection between the different models. This is done by calculating the Digital Elevation Model of Differences (DoD) using the OPALS module Diff (Pfeifer et al., 2014). Here, changes are computed from the two input surface grid models of different epochs, which then identify height changes within a set grid size. The DoD models were calculated with a grid size of 1 m and otherwise run with standard parameters. This workflow is now applied to first obtain the vegetation height of each epoch by computing the DoD for the Winter 2024/2025 DTM and each DSM. Secondly, the vegetation DSMs can be compared for different seasons to analyze changes throughout normal seasonality. Lastly, the DSMs of the year before and after the flood are compared to analyze the impact of the flood on the pond.

4. Results

The previously introduced workflow is now applied to each epoch's DSM. This yields the vegetation height for each measurement and, furthermore, allows us to compare seasonal changes and the flood-induced changes.

4.1 Vegetation extent

The results of the proposed analysis clearly show the vast vegetation extent before the flood and an almost undetectable remainder after the event (Figure 2). For the first four epochs, the vegetation fluctuates in a seasonal circle between the half-yearly intervals. With the largest extent in autumn 2023 (Figure 2C and Figure 4C) and the smallest in Winter 2022/2023 (Figure 2B and Figure 4B). Furthermore, the ROV images shown in Figure 2A confirm an overall vast vegetation height and extent for the pond in Spring 2024. For the first measurement after the flood event in autumn 2024, there is no vegetation detectable in the pond (Figure 4E). This is the first indicator that the extent of the vegetation has changed, as in the years before the flood, vegetation was visible in this period of the year (Figures 4A and C). However, for this epoch, the turbidity of the pond exceeds previous surveys, as no bottom echoes could be extracted due to suspended sediment in the pond after the flood (Figure 3E). For the last epoch, the pond shows again some vegetation, which is located mainly around 0 m to 50 m (East) and 200 m (North). There, the small island in the pond might have shielded the vegetation to some extent, since the flood was flowing in the northwest direction. However, with a reasonable depth covered, due to the usage of a lower flight altitude and

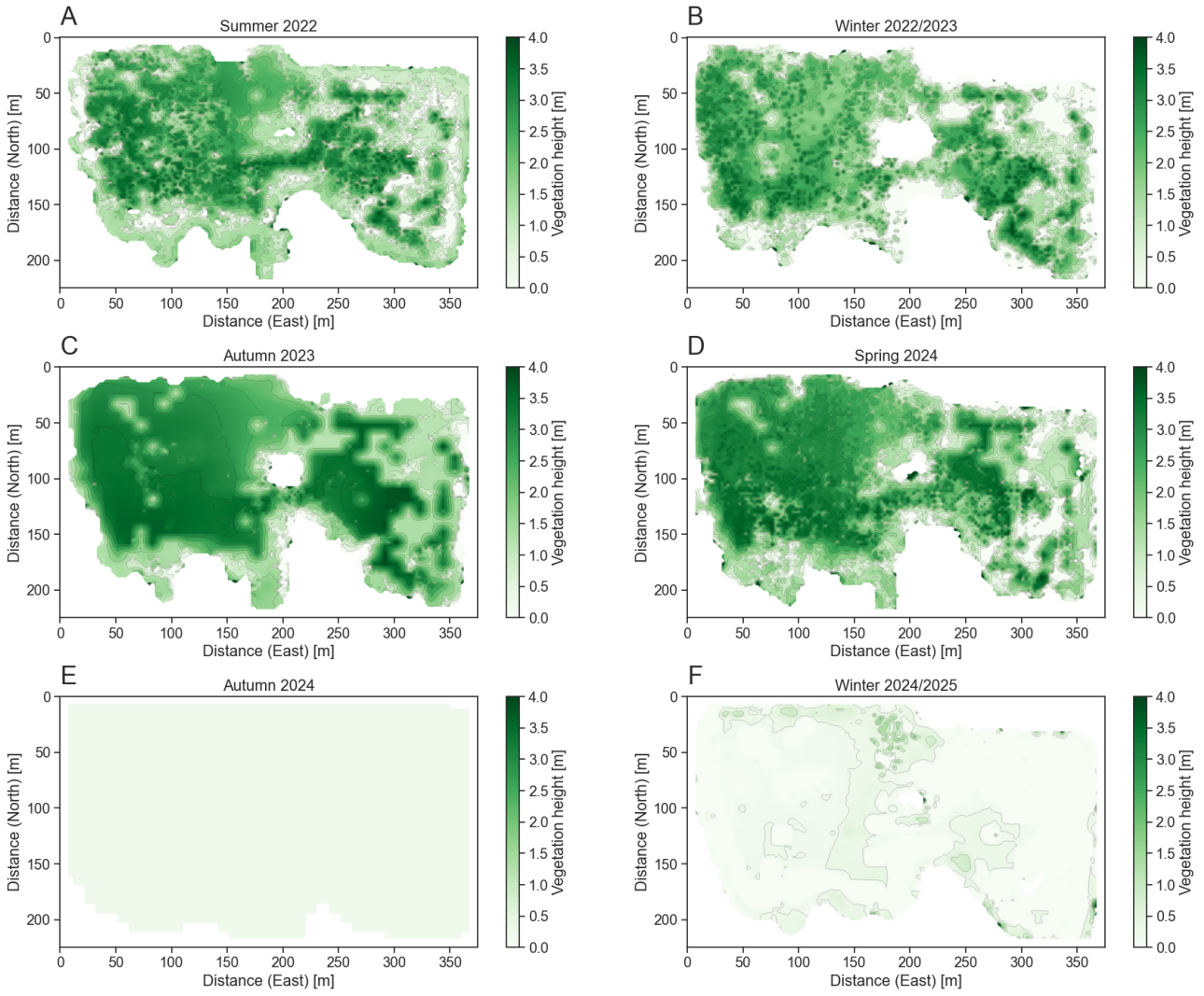

Figure 4. Vegetation height for each LiDAR epoch based on the difference between the epoch DSM and the Winter 2024/2025 DTM. Panels A-D show the vegetation height before the flood and panels E and F display the vegetation height after.

a different scanner, the remaining vegetation can be accurately mapped, indicating a significant reduction compared to previous years.

4.2 Seasonal vegetation changes

To extend the analysis from vegetation height maps to seasonal change detection, we analyze the DoDs (Section 3.3) between consecutive epochs before the flood event. This yields three periods of approximately half a year in which the vegetation underwent seasonal changes. These changes can be seen in Figure 5. There, seasonal changes are in alignment with the expected results, as a decrease from summer or fall to winter is visible (Figure 5A and C) and an increase during the winter to autumn period (Figure 5B). During each seasonal change, the vegetation neither completely vanishes nor sprouts without prior presence, which is typical for the type of macrophytes found in the surveyed pond (*Characeae*). Furthermore, the recorded vegetation height is highest during summer and autumn (Figure 4) and a lower but stable coverage remains during winter (Figure 4). Thus, most observable changes fall within the $\pm 2\,\mathrm{m}$ range.

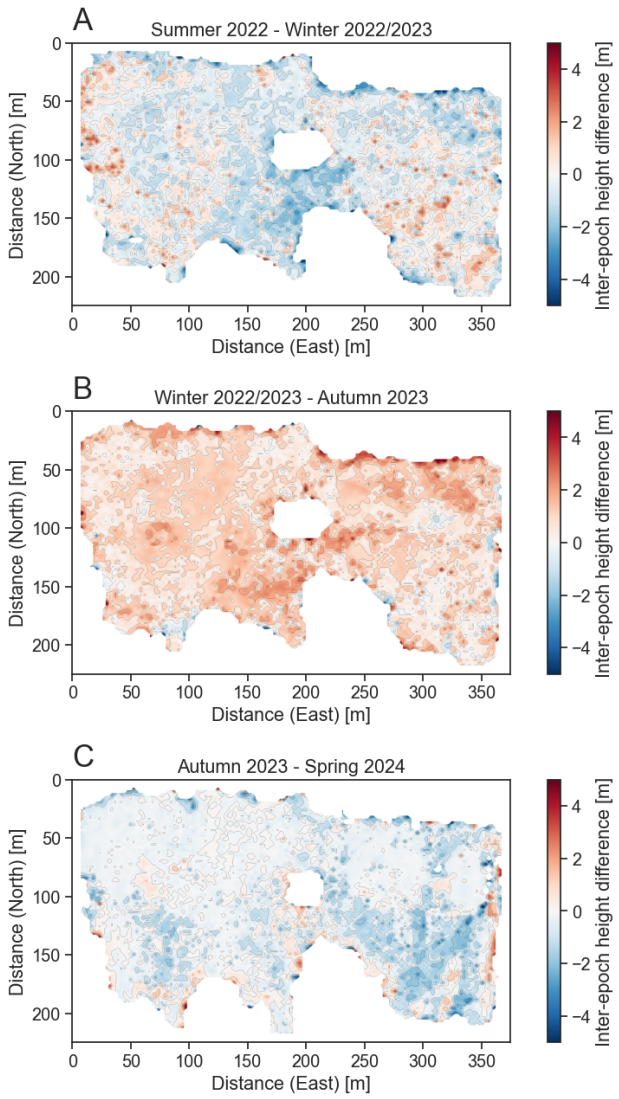

Figure 5. Seasonal changes before the September 2024 flood. Each panel displays an approximately half year period.

4.3 Flood induced changes in vegetation

In Figure 6 we show the last period before the flood and the first after the flood. A drastic change in vegetation height can be seen between both epochs. For most of the pond, a large negative change in vegetation height can be seen (Figure 6 B). The only exception to this is the vegetation near $0\,\mathrm{m}$ to $50\,\mathrm{m}$ (East) and $200\,\mathrm{m}$ (North). However, for the remaining vegetation, there was a decrease in height. Compared to a similar period between 2023 and 2024 (Figure 6 A), where vegetation increased due to the onset of spring.

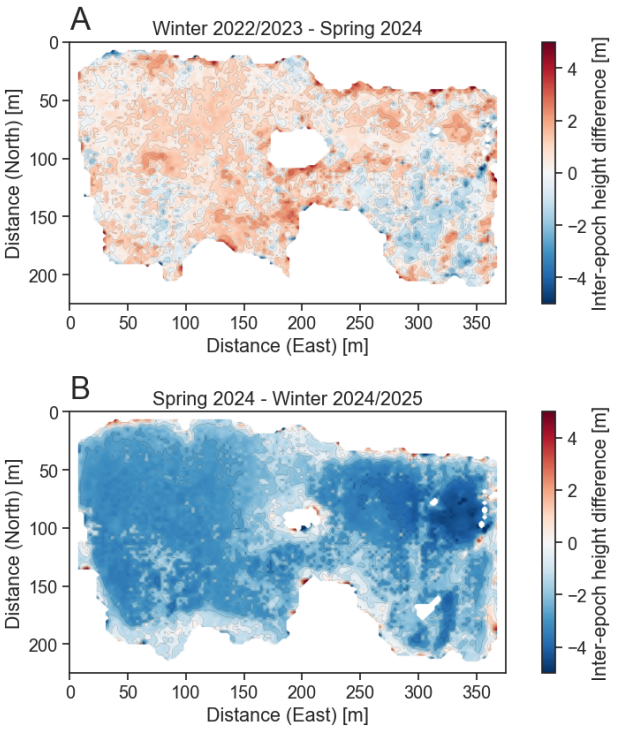

Figure 6. Change detection for the year before the flood and the year during the flood.

5. Discussion

The documented vegetation changes highlight the importance of continuous monitoring of aquatic ecosystems. For these, the flood event displays a local extinction event and irrevocably alters the pond ecosystem. To relate these changes with current ecological research, this section discusses these topics in light of the acquired insights.

5.1 Vegetation height estimation

For both, the change detection and vegetation height estimation, the DSMs are based on the maximum height within each grid cell, which, depending on the point cloud density and general noise, is susceptible to outliers. Through the cross-section plots (Figure 3), we can see that this is not necessarily the case for the selected data set as the point cloud displays uniform coverage with the only exception being the Spring 2024 data set, where the point density is lower, but the height of the vegetation remains continuous. Thus, the aspect of outliers that determine the height of the DSM can be neglected.

Another factor to consider for the estimation of the vegetation height in Section 4.1, is that due to the sparse detection

of the terrain for multiple different epochs, the terrain of the last epoch was used. There, the assumption that the terrain has not changed over the three years represents a weak assumption; an alternative here would be rough interpolation which might introduce large inaccuracies. For measurements during winter and while the vegetation has not reached the surface, a detailed terrain model would be achievable. However, this would not work for the summer and autumn periods as there the floating vegetation leads to almost no bottom echos throughout the whole pond. Thus, the results are comparable in height, but might not represent the height of the epoch to the truest from, as there is potential variation. Improved DTMs for each epoch could potentially be achieved by analyzing differences between the recorded terrain of each epoch and using yearly terrain models based on merged terrain data.

Lastly, the height and change of vegetation between seasons can be compared to the literature, since previous studies have analyzed the changes in vegetation through in situ surveys (Kotta et al., 2021; Rip et al., 2007). The results of our study show an overall alignment with the moderate decrease and increase during the observed intervals (Kotta et al., 2021), furthermore suggesting the suitability of repeated optical remote sensing to survey aquatic vegetation.

5.2 Ecological impact of the flood event

The flood event significantly influenced the extent and height of the vegetation for the remaining vegetation population. Along with this change, an increased turbidity of the pond was observed, which persists even after the flood receded in the generally clearest period of the pond during the winter (Figure 2F). This aligns well with the literature that mentions a decrease in turbidity through the presence of macrophytes (Gomes et al., 2024; Scheffer, 1999; Scheffer and van Nes, 2007), which now leads, after the near-extinction of macrophytes, to turbid conditions. This in turn negatively impacts vegetation coverage through reduced sunlight (Austin et al., 2017).

A secondary factor is the introduction of new fish populations through the temporary connection to neighboring ponds (Carlson et al., 2016; Casimiro et al., 2018). Throughout previous studies, no notable fish populations were observed before the 2024 flood event. In the last epoch, during field work, large carp could be observed at multiple locations of the pond, suggesting an introduction of the fish through the flood event. Although the literature suggests that hydrological changes are the main influence on water turbidity (Fletcher et al., 1985), there is evidence that fish play a role in vegetation reduction and thus can indirectly affect water turbidity (Fletcher et al., 1985; Richardson et al., 1995; Kloskowski, 2011). Therefore, the pond ecosystem might be altered, with reduced vegetation and increased turbidity, for an unknown amount of time. In addition to the biological impact, this furthermore worsens the measurability, since the increase in turbidity decreases the achievable depth penetration of bathymetric LiDAR and thus limits future studies on the ecological impact.

6. Conclusion

The study investigated the topic of macrophyte seasonality using optical hydrography (aerial imagery and bathymetric LiDAR) and analyzed the impact of flood events on macrophytes in a small-scale case study that highlights the influence of extreme weather events on aquatic vegetation. The results show a significant decrease in vegetation coverage and a near-extinction event for the macrophyte population of the surveyed pond. In addition to vegetation changes, the introduction of fish through the flood further impacts the ecosystem. Based on the results of the analysis, this indicates a long-term change in the ecosystem of the pond. With an increase in turbidity, both the ecosystem as well as the LiDAR penetration depth have been altered, and thus future investigations of the ecological impact could potentially be limited. However, we show that optical remote sensing methods and bathymetric LiDAR in particular can be used to monitor the vegetation of submerged ecosystems. Thus, airborne laser bathymetry has proven to be a cost-effective technique to monitor vital data for ecological research.

References

Austin, N., Hansen, J. P., Donadi, S., Eklöf, J. S., 2017. Relationships between aquatic vegetation and water turbidity: A field survey across seasons and spatial scales. *PLOS ONE*, 12(8), e0181419.

BEV, B. f. E.-u. V., 2024. Austrian map online. https://www.bev.gv.at/Services/Produkte/Austrian-Map/Austrian-Map-online.html.

Blöschl, G., 2024. September 2024 flooding in Central Europe: The Austrian experience. {https://blogs.egu.eu/geolog/2024/09/26/september-2024-flooding-in-central-europe-the-austrian-experience}. EGU Blogs, GeoLog.

Blöschl, G., Blaschke, A. P., Haslinger, K., Hofstätter, M., Parajka, J., Salinas, J., Schöner, W., 2018. Auswirkungen der Klimaänderung auf Österreichs Wasserwirtschaft – ein aktualisierter Statusbericht. *Österreichische Wasser- und Abfallwirtschaft*, 70(9–10), 462–473.

Carlson, A. K., Fincel, M. J., Longhenry, C. M., Graeb, B. D., 2016. Effects of historic flooding on fishes and aquatic habitats in a Missouri River delta. *Journal of Freshwater Ecology*, 31(2), 271–288.

Casimiro, A. C. R., Garcia, D. A. Z., Vidotto-Magnoni, A. P., Britton, J. R., Agostinho, A. A., De Almeida, F. S., Orsi, M. L., 2018. Escapes of non-native fish from flooded aquaculture facilities: the case of Paranapanema River, southern Brazil. *Zoologia*, 35, 1–6.

Chabot, D., Dillon, C., Shemrock, A., Weissflog, N., Sager, E. P. S., 2018. An Object-Based Image Analysis Workflow for Monitoring Shallow-Water Aquatic Vegetation in Multispectral Drone Imagery. *ISPRS International Journal of Geo-Information*, 7(8), 294.

Eriksson, B., Sandström, A., Isæus, M., Schreiber, H., Karås, P., 2004. Effects of boating activities on aquatic vegetation in the Stockholm archipelago, Baltic Sea. *Estuarine, Coastal and Shelf Science*, 61(2), 339–349.

Fletcher, A., Morison, A., Hume, D., 1985. Effects of carp, Cyprinus carpio L., on communities of aquatic vegetation and turbidity of waterbodies in the lower Goulburn River basin. *Marine and Freshwater Research*, 36(3), 311–327.

Gomes, P. C. S., Rochinha, I. d. S. P., Paiva, M. H. R. d., Santiago, A. d. F., 2024. Performance of Different Macrophytes and Support Media in Constructed Wetlands for High Turbidity Reduction from Mine Spoil Rainwater. *Resources*, 13(12), 168.

Hollaus, M., Mandlburger, G., Pfeifer, N., Mücke, W., 2010. Land cover dependent derivation of digital surface models from airborne laser scanning data. *IAPRS*, 38, 1–3.

Kellaris, A., Gil, A., Faria, J., Amaral, R., Moreu-Badia, I., Neto, A., Yesson, C., 2019. Using low-cost drones to monitor heterogeneous submerged seaweed habitats: A case study in the Azores. *Aquatic Conservation: Marine and Freshwater Ecosystems*, 29(11), 1909–1922.

Kloskowski, J., 2011. Impact of common carp Cyprinus carpio on aquatic communities: direct trophic effects versus habitat deterioration. *Fundamental and Applied Limnology-Archiv furHydrobiologie*, 178(3), 245.

Kotta, J., Torn, K., Paalme, T., Rätsep, M., Kaljurand, K., Teeveer, M., Kotta, I., 2021. Scale-Specific Patterns of the Production of the Charophyte Chara aspera in the Brackish Baltic Sea: Linking Individual and Community Production and Biomass Growth. *Frontiers in Marine Science*, 8.

Lønborg, C., Thomasberger, A., Stæhr, P. A. U., Stockmarr, A., Sengupta, S., Rasmussen, M. L., Nielsen, L. T., Hansen, L. B., Timmermann, K., 2021. Submerged aquatic vegetation: Overview of monitoring techniques used for the identification and determination of spatial distribution in European coastal waters. *Integrated Environmental Assessment and Management*, 18(4), 892–908.

Mader, D., Richter, K., Westfeld, P., Maas, H.-G., 2021. Potential of a Non-linear Full-Waveform Stacking Technique in Airborne LiDAR Bathymetry: Demonstration of Full-Waveform Stacking Techniques on Data from the Elbe River. *PFG–Journal of Photogrammetry, Remote Sensing and Geoinformation Science*, 89(2), 139–158.

Mandlburger, G., 2022. A review of active and passive optical methods in hydrography. *The International Hydrographic Review*, 8–52.

Mandlburger, G., Hauer, C., Wieser, M., 2013. Monotoring of instream habitats with focus on morphological dynamics based on Airborne Laser Bathymetry.

Mandlburger, G., Hauer, C., Wieser, M., Pfeifer, N., 2015. Topo-bathymetric LiDAR for monitoring river morphodynamics and instream habitats—A case study at the Pielach River. *Remote Sensing*, 7(5), 6160–6195.

Mandlburger, G., Pfennigbauer, M., Schwarz, R., Pöppl, F., 2023. A decade of progress in topo-bathymetric laser scanning exemplified by the pielach river dataset. *ISPRS Annals of the Photogrammetry, Remote Sensing and Spatial Information Sciences*, 10, 1123–1130.

Murphy, F., Schmieder, K., Baastrup-Spohr, L., Pedersen, O., Sand-Jensen, K., 2018. Five decades of dramatic changes in submerged vegetation in Lake Constance. *Aquatic Botany*, 144, 31–37.

Ostendorp, W., Dienst, M., Schmieder, K., 2003. Disturbance and rehabilitation of lakeside Phragmites reeds following an extreme flood in Lake Constance (Germany). *Hydrobiologia*, 506, 687–695.

Pfeifer, N., Mandlburger, G., Otepka, J., Karel, W., 2014. OPALS – A framework for Airborne Laser Scanning data analysis. *Computers, Environment and Urban Systems*, 45, 125–136.

Pfennigbauer, M., Ullrich, A., Schwarz, R., 2020. Waveform-averaging airborne laser bathymetry scanner. M. D. Turner, G. W. Kamerman (eds), *Laser Radar Technology and Applications XXV*, SPIE, 19.

Rhomberg-Kauert, J., Dammert, L., Grömer, M., Pfennigbauer, M., Mandlburger, G., 2024. Macrophyte detection with bathymetric LiDAR – Applications of high-dimensional data analysis for submerged ecosystems. *The International Hydrographic Review*, 30(2), 98–115.

Richardson, M. J., Whoriskey, F. G., Roy, L. H., 1995. Turbidity generation and biological impacts of an exotic fish Carassius auratus, introduced into shallow seasonally anoxic ponds. *Journal of Fish Biology*, 47(4), 576–585.

Rip, W. J., Ouboter, M. R. L., Los, H. J., 2007. Impact of climatic fluctuations on Characeae biomass in a shallow, restored lake in The Netherlands. *Hydrobiologia*, 584(1), 415–424.

Rowan, G. S. L., Kalacska, M., 2021. A Review of Remote Sensing of Submerged Aquatic Vegetation for Non-Specialists. *Remote Sensing*, 13(4), 623.

Scheffer, M., 1999. *The effect of aquatic vegetation on turbidity; how important are the filter feeders?* Springer Netherlands, 307–316.

Scheffer, M., van Nes, E. H., 2007. Shallow lakes theory revisited: various alternative regimes driven by climate, nutrients, depth and lake size. *Hydrobiologia*, 584(1), 455–466.

Schmieder, K., Dienst, M., Ostendorp, W., n.d. Auswirkungen des Extremhochwassers 1999 auf die Flächendynamik und Bestandsstruktur der Uferröhrichte des Bodensees Effects of the extreme flood in 1999 on the spatial dynamics and stand structure of the reed belts in Lake Constance.

Schumacher, J., Horn, D., Escobar-Sánchez, G., Markfort, G., Schernewski, G., von Weber, M., 2024. Assessing Macrophyte and Ecosystem Service Changes in Shallow Eutrophic Coastal Waters Using Remote Sensing Methods. *Land*, 14(1), 4.

Schwarz, R., Mandlburger, G., Pfennigbauer, M., Pfeifer, N., 2019. Design and evaluation of a full-wave surface and bottom-detection algorithm for LiDAR bathymetry of very shallow waters. *ISPRS journal of photogrammetry and remote sensing*, 150, 1–10.

Schwarz, R., Pfeifer, N., Pfennigbauer, M., Ullrich, A., 2017. Exponential decomposition with implicit deconvolution of lidar backscatter from the water column. *PFG–Journal of Photogrammetry, Remote Sensing and Geoinformation Science*, 85, 159–167.

Ventura, D., Bonifazi, A., Gravina, M. F., Ardizzone, D. et al., 2017. Unmanned aerial systems (uass) for environmental monitoring. a review with applications in coastal habitats. *Aerial Robots. Aerodynamics, control and applications*, InTech Open, 165–183.

Wagner, N., Franke, G., Schmieder, K., Mandlburger, G., 2024. Automatic Classification of Submerged Macrophytes at Lake Constance Using Laser Bathymetry Point Clouds. *Remote Sensing*, 16(13), 2257.